

Flux vector formulation for photon propagation in the biological tissue

W. Cong,* A. Cong, H. Shen, Y. Liu, and G. Wang¹

Biomedical Imaging Division, School of Biomedical Engineering and Sciences, Virginia Polytechnic Institute and State University, 1880 Pratt Drive, Blacksburg, Virginia 24061, USA

¹wangg@vt.edu

*Corresponding author: congw@vt.edu

Received July 5, 2007; revised August 23, 2007; accepted August 28, 2007; posted August 30, 2007 (Doc. ID 84861); published September 25, 2007

We present a generalized delta-Eddington phase function to simplify the radiative transfer equation to an integral equation with respect to the photon flux vector. The solution of the integral equation is highly accurate to model the photon propagation in the biological tissue over a broad range of optical parameters, especially in the visible light spectrum where the diffusion approximation breaks down. The methodology is validated in the Monte Carlo simulation and can be applied in various optical imaging applications. © 2007 Optical Society of America

OCIS codes: 170.3660, 170.3880.

The diffusion approximation (DA) to the radiative transfer equation (RTE) has been widely used to describe the photon propagation in the biological tissue because of its high computational efficiency. However, the DA is based on the assumption of weakly anisotropic scattering and only works well in low absorbing and highly scattering media [1,2]. These conditions seriously limit the utility of the DA, especially in the emerging molecular optical imaging areas such as bioluminescence and fluorescence imaging [3]. Quantitative imaging of bioluminescent markers and fluorescent proteins, which are characterized in the spectral range of 400–600 nm, involve higher photon absorption in the biological tissue compared with the near-infrared (NIR) imaging schemes, rendering the DA quite problematic [4,5]. In this Letter, we propose a generalized delta-Eddington phase function to address this challenge. Using the new phase function to simplify the RTE, the photon flux vector is, for the first time to our knowledge, formulated as a solution of an integral equation. Photon flux describes the axial photon energy transfer and is directly related to experimental measurement data on the boundary [2], which has practical significance for the optical imaging.

The RTE describes the variation of the photon radiance $L(\mathbf{r}, \mathbf{s})$ at position \mathbf{r} and along the solid direction \mathbf{s} in the biological tissue [1,2]:

$$[\mathbf{s} \cdot \nabla + (\mu_a + \mu_s)]L(\mathbf{r}, \mathbf{s}) = \mu_s \oint_{4\pi} L(\mathbf{r}, \mathbf{s}')p(\mathbf{s}, \mathbf{s}')d\mathbf{s}' + \frac{1}{4\pi}Q(\mathbf{r}), \quad \mathbf{r} \in \Omega, \quad (1)$$

where Ω is the region of interest, $Q(\mathbf{r})$ is the isotropic light source, μ_s is the scattering coefficient, and μ_a is the absorption coefficient. The scattering phase function $p(\mathbf{s}, \mathbf{s}')$ gives the probability of photons coming in the direction \mathbf{s}' that is scattered into the direction \mathbf{s} . The biological tissue scatters light strongly in the forward direction, and the scattering phase function can be modeled by a generalized delta-Eddington function [2,6]:

$$p(\mathbf{s}, \mathbf{s}') = \frac{1}{4\pi}[(1-f)(1+3h\mathbf{s} \cdot \mathbf{s}') + 2f\delta(1-\mathbf{s} \cdot \mathbf{s}')], \quad (2)$$

where $f \in [-1, 1]$ is the weight factor measuring the anisotropy of photon scattering, which we call the anisotropy weight, and h is the asymmetry factor. The generalized phase function is a linear combination between the weakly isotropic scattering and the strongly peaked forward scattering. The original delta-Eddington phase function rigidly defines f as a fixed value g^2 , and h as $g/(1+g)$, where g is an anisotropic factor defined as the mean of the cosine of the scattering angles [6]. In contrast to these conventional interpretations, our generalized delta-Eddington function requires that the anisotropy weight and asymmetry factor are related to the photon absorbing and scattering in the tissue and can be determined by Monte Carlo (MC) simulation from known absorption coefficient, scattering coefficient, and anisotropic factor. As a result, the optical properties of the medium are now characterized by absorption coefficient, scattering coefficient, anisotropy weight, and asymmetry factor, which can also be determined by the diffuse optical tomography (DOT)-like optical tomography techniques [7].

Substituting Eq. (2) into Eq. (1), we have

$$(\mathbf{s} \cdot \nabla + \tilde{\mu}_t)L(\mathbf{r}, \mathbf{s}) = \frac{\tilde{\mu}_s}{4\pi}[\Phi(\mathbf{r}) + 3h\mathbf{s} \cdot \mathbf{J}(\mathbf{r})] + \frac{1}{4\pi}Q(\mathbf{r}), \quad (3)$$

where $\tilde{\mu}_s = (1-f)\mu_s$, $\tilde{\mu}_t = \tilde{\mu}_s + \mu_a$, $\Phi(\mathbf{r})$ is the photon fluence rate, and $\mathbf{J}(\mathbf{r})$ is the photon flux vector. Furthermore, the integration of Eq. (1) over all the 4π solid angle leads to

$$\nabla \cdot \mathbf{J}(\mathbf{r}) + \mu_a\Phi(\mathbf{r}) = Q(\mathbf{r}), \quad \mathbf{r} \in \Omega. \quad (4)$$

Substituting Eq. (4) into Eq. (3), we have

$$(\mathbf{s} \cdot \nabla + \tilde{\mu}_t)L(\mathbf{r}, \mathbf{s}) = \frac{1}{4\pi}\beta(\mathbf{r})(3h\mu_a\mathbf{s} - \nabla) \cdot \mathbf{J}(\mathbf{r}) + \frac{1}{4\pi}[1 + \beta(\mathbf{r})]Q(\mathbf{r}), \quad (5)$$

where $\beta(\mathbf{r}) = \tilde{\mu}_s(\mathbf{r})/\mu_a(\mathbf{r})$. Equation (5) is a linear, first-order differential equation describing the photon propagation in a heterogeneous media, and $L(\mathbf{r}, \mathbf{s})$ can be formulated as [8]

$$L(\mathbf{r}, \mathbf{s}) = -\frac{1}{4\pi} \int_0^R [\beta(\mathbf{r} - \rho\mathbf{s})(3h\mu_a\mathbf{s} + \nabla) \cdot \mathbf{J}(\mathbf{r} - \rho\mathbf{s}) - (1 + \beta(\mathbf{r} - \rho\mathbf{s}))Q(\mathbf{r} - \rho\mathbf{s})]w(\rho, \mathbf{r}, \mathbf{s})d\rho + L(\mathbf{r} - R\mathbf{s}, \mathbf{s})w(R, \mathbf{r}, \mathbf{s}), \quad (6)$$

where $w(x, \mathbf{r}, \mathbf{s}) = \exp(-\int_0^x \tilde{\mu}_t(\mathbf{r} - t\mathbf{s})dt)$, and R is a scalar so that $\mathbf{r} - R\mathbf{s} \in \partial\Omega$. $L(\mathbf{r} - R\mathbf{s}, \mathbf{s})$ in Eq. (6) describes the photons entering into tissues along the direction \mathbf{s} on the boundary. While no external photon travels in an inward direction on the boundary, $L(\mathbf{r} - R\mathbf{s}, \mathbf{s})$ would vanish for matched refractive indices on the boundary. However, since the refractive index of the biological tissue is higher than the refractive index of the surrounding air, a fraction of photons will be internally reflected at the boundary. In this case, $L(\mathbf{r} - R\mathbf{s}, \mathbf{s})$ represents the contribution from reflected photons on the boundary. From Fresnel laws, the reflected radiance $L(\mathbf{r} - R\mathbf{s}, \mathbf{s})$ on the boundary is expressed as

$$L(\mathbf{r} - R\mathbf{s}, \mathbf{s}) = r_d L(\mathbf{r} - R\mathbf{s}, \mathbf{s}'), \quad \mathbf{s} \cdot \mathbf{n} < 0, \quad (7)$$

where $\mathbf{s}' = \mathbf{s} - 2(\mathbf{s} \cdot \mathbf{n})\mathbf{n}$, \mathbf{n} is the outward unit normal at $\mathbf{r} - R\mathbf{s}$ on $\partial\Omega$, and r_d the internal reflection coefficient [5,9]. In terms of the boundary condition of diffusion approximation $\Phi(\mathbf{r}) = 2A\mathbf{J}(\mathbf{r}) \cdot \mathbf{n}$, $\mathbf{r} \in \partial\Omega$ [9,10], the reflected radiance $L(\mathbf{r} - R\mathbf{s}, \mathbf{s})$ on the boundary can be approximated by

$$L(\mathbf{r} - R\mathbf{s}, \mathbf{s}) \approx \frac{r_d}{4\pi} \mathbf{J}(\mathbf{r} - R\mathbf{s}) \cdot [3\mathbf{s} + (2A - 6\mathbf{n} \cdot \mathbf{s})\mathbf{n}], \quad (8)$$

where A is a coefficient depending on the relative refractive index mismatch between the tissue and surrounding air [9]. Substituting Eq. (8) into Eq. (6), multiplying both sides of Eq. (6) by the unit vector \mathbf{s} , integrating over the 4π solid angle of \mathbf{s} , and performing a variable transformation from the polar coordinates $\mathbf{r} - \rho\mathbf{s}$ to the Cartesian coordinates \mathbf{r}' , we obtain an integral equation for the photon flux vector:

$$\mathbf{J}(\mathbf{r}) = -\frac{1}{4\pi} \int_{\Omega} [\beta(\mathbf{r}')(\nabla + 3h\mu_a\mathbf{v}) \cdot \mathbf{J}(\mathbf{r}') - (1 + \beta(\mathbf{r}'))Q(\mathbf{r}')]G(\mathbf{r}, \mathbf{r}')\mathbf{v}d\mathbf{r}' - \frac{r_d}{4\pi} \oint_{\partial\Omega} [3\mathbf{v} + (2A - 6\mathbf{n} \cdot \mathbf{v})\mathbf{n}] \cdot \mathbf{J}(\mathbf{r}')G(\mathbf{r}, \mathbf{r}')(\mathbf{n} \cdot \mathbf{v})\mathbf{v}d\mathbf{r}', \quad (9)$$

where $\mathbf{v} = (\mathbf{r} - \mathbf{r}')/|\mathbf{r} - \mathbf{r}'|$, $G(\mathbf{r}, \mathbf{r}') = w(|\mathbf{r} - \mathbf{r}'|, \mathbf{r}, \mathbf{v})/|\mathbf{r} - \mathbf{r}'|^2$. For simplicity, we call Eq. (9) the phase approximation (PA) equation because it is derived from an approximate phase function. Equation (9) is a well-posed integral equation of the second kind for the photon flux vector and allows an accurate description of the photon propagation in the biological tissue. The detector readings on the boundary are derivable from the exiting partial current $\Gamma(\mathbf{r}) = \oint_{\mathbf{s} \cdot \mathbf{n} > 0} \mathbf{s}L(\mathbf{r}, \mathbf{s})d\mathbf{s}$, $\mathbf{r} \in \partial\Omega$, while $\Gamma(\mathbf{r})$ is related to the photon flux: $\Gamma(\mathbf{r}) = \mathbf{J}(\mathbf{r}) \cdot \mathbf{n}/(1 - r_d)$, $0 < r_d < 1$, $\mathbf{r} \in \partial\Omega$ [2].

To perform the numerical computation, Eq. (9) can be discretized into a matrix equation [11]:

$$\{\mathbf{J}\} = \mathbf{M}\{\mathbf{J}\} + \{\mathbf{Q}\}, \quad (10)$$

where \mathbf{M} and $\{\mathbf{Q}\}$ represent the corresponding discrete integral kernels and source vector in Eq. (9). Equation (10) can be solved numerically to compute the photon flux $\{\mathbf{J}\}$. Extensive numerical experiments were conducted to evaluate the proposed method. In our experiments, a spherical phantom of radius 10 mm was first used to determine the anisotropy weight f and asymmetry factor h based on the known absorption, scattering coefficients, and anisotropic factor g . A spherical source of radius 0.6 mm was embedded into the spherical phantom with its center at (2.5, 2.5, 0.0). The phantom was discretized into tetrahedral elements with an average edge of 0.8 mm. A total of 2108 virtual detectors were distributed on the phantom surface to record the photon flux. The MC simulation with Henyey-Greenstein phase function was performed from the known optical parameters (μ_a , μ_s , g , and η) to obtain the exiting partial current on the detectors. Then, the anisotropy weight f and asymmetry factor h were determined by matching the exiting partial current obtained from the PA equation (9) to the exiting partial current data generated by the MC simulation. The procedure was run on three sets of optical parameters with various values of the relative reduced scattering coefficient (RRSC) defined by $\mu_s(1-g)/\mu_a$ to compute the anisotropy weight and asymmetry factor, respectively. The computed results were shown in Table 1. Furthermore, a cylindrical phantom of diameter 20 mm and height 20 mm was employed to compare the accuracy between the MC simulation and PA and DA models. A spherical source of radius 1.0 mm was embedded into the phantom with its center at (-4.0, 0.0, 10.0). The phantom was discretized into 25,335 tetrahedral elements and 4833 nodes for the numerical computation of the PA and DA models. A total of 1226 virtual de-

Table 1. Optical Parameters Used in the Simulation

μ_a (mm ⁻¹)	μ_s (mm ⁻¹)	g	η	f	h
0.35	12.50	0.9	1.37	0.917	0.90
0.20	14.50	0.9	1.37	0.940	0.92
0.016	9.0	0.9	1.37	0.967	0.95

tectors were allocated on the phantom surface to record the exiting partial current and fluence rate. Our in-house numerical simulator was executed to generate the exiting partial current on the boundary of the phantom based on the MC and PA models, respectively, with the three sets of the optical parameters in Table 1. Figures 1(a), 1(c), and 1(e) present the comparison between the solution of the PA and MC simulations for RRSC 3.57, 7.25, and 56.25, respectively. The results show that the solutions obtained from the PA were in excellent agreement with the results from the MC simulation with a relative error of $\sim 5.0\%$. In contrast, we performed the numerical experiments with same phantom setting based on the DA model. As a result, the relative errors between the solutions of the DA and MC simulations were as high as 31.2% and 14.6% for RRSC 3.57 and 7.25, respectively, as shown in Figs. 1(b) and 1(d). As is expected, the DA model worked well with relative errors below 5.0% for RRSC of 56.25, as shown in Fig. 1(f). The numerical experiments show that the solutions obtained from the PA equation are consistently more accurate than the results from the DA model relative to the MC simulation data. The anisotropy weight f and asymmetry factor h are independent of the geometrical shape of the medium and are the critical parameters to describe the optical properties of the medium. Furthermore, the compu-

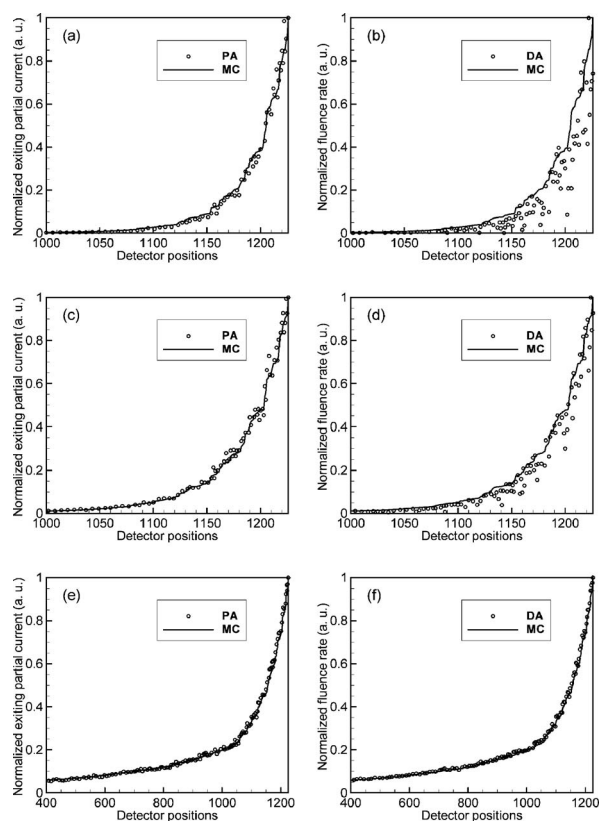


Fig. 1. Comparison between the MC simulation and PA and DA models with the optical parameters $\mu_a = 0.35 \text{ mm}^{-1}$, $\mu_s = 12.5 \text{ mm}^{-1}$, $h = 0.9$, and $f = 0.917$ for (a), (b); $\mu_a = 0.20 \text{ mm}^{-1}$, $\mu_s = 14.5 \text{ mm}^{-1}$, $h = 0.92$, and $f = 0.94$ for (c), (d); and $\mu_a = 0.016 \text{ mm}^{-1}$, $\mu_s = 9.0 \text{ mm}^{-1}$, $h = 0.95$, and $f = 0.967$ for (e), (f). The detector positions were sorted according to increasing order of MC data.

tational cost of the PA model is much lower than that of the MC simulation. For example, the computational time of the PA model was ~ 15 min in our numerical experiments, while that of the MC simulation with the photon number of 10^7 was ~ 80 min, and that of the DA model in the same setting was ~ 3 min.

In summary, we have presented a generalized delta-Eddington phase function, which is characterized by anisotropy weight and asymmetry factor. Compared with the original delta-Eddington phase function that fixes the anisotropy weight to g^2 and the asymmetry factor to $g/(1+g)$, our proposed generalized delta-Eddington phase function requires that the anisotropy weight and asymmetry factor relate to the photon absorbing and scattering coefficients of the biological tissue and can be obtained in the MC simulation from known absorption, scattering coefficients, and conventional anisotropic factor g . In this way, the optical properties of the medium can be characterized by absorption, scattering coefficients, the anisotropy weight, and the asymmetry factor, which can also be determined using a DOT-like optical tomography technique. Using the generalized delta-Eddington phase function, the radiative equation has been greatly simplified into an integral equation with respect to the photon flux. Different from the DA model derived from the first-order approximation of the photon radiance, the PA model is based on the exact calculation of the photon radiance inside the biological tissue, with the DA for the photon radiance on boundary. The numerical experiments have demonstrated that the solution of the PA equation is highly accurate over a broad range of optical parameters relative to the MC simulation data. The proposed methodology has great potential for biomedical optical imaging, especially bioluminescence and fluorescence imaging.

This work was partially supported by the National Institutes of Health under grants EB001685, EB006036, and CA127189.

References

1. A. Ishimaru, *Wave Propagation and Scattering in Random Media* (Academic, 1978), Vol. 1.
2. A. J. Welch and M. J. C. van Gemert, *Optical and Thermal Response of Laser-Irradiated Tissue* (Plenum, 1995).
3. C. H. Contag and M. H. Bachmann, *Annu. Rev. Biomed. Eng.* **4**, 235 (2002).
4. J. Ripoll, D. Yessayan, G. Zacharakis, and V. Ntziachristos, *J. Opt. Soc. Am. A* **22**, 546 (2005).
5. A. D. Klose and E. W. Larsen, *J. Comput. Phys.* **220**, 441 (2006).
6. J. H. Joseph, W. J. Wiscombe, and J. A. Weinman, *J. Atmos. Sci.* **33**, 2452 (1976).
7. S. R. Arridge, *Inverse Probl.* **15**, R41 (1999).
8. F. Natterer and F. Wubbeling, *Mathematical Methods in Image Reconstruction* (SIAM, 2001).
9. M. Keijzer, W. M. Star, and P. R. M. Storchi, *Appl. Opt.* **27**, 1820 (1988).
10. R. A. J. Groenhuis, H. A. Ferwerda, and J. J. Ten Bosch, *Appl. Opt.* **22**, 2456 (1983).
11. S. S. Rao, *The Finite Element Method in Engineering* (Butterworth-Heinemann, 1999).